

Influence of Control Strategy in Risk Mitigation of Building Damage Due to Earthquake

Normaisharah Mamat (✉ normysarahmn@gmail.com)

Universiti Teknologi Malaysia <https://orcid.org/0000-0002-6502-5327>

Mohd Fauzi Othman

Universiti Teknologi Malaysia

Mohd Fitri Mohd Yakub

Universiti Teknologi Malaysia

Research Article

Keywords: Control strategy. Deep learning. Collapse probability. Building damage. Enhance building safety

Posted Date: September 27th, 2021

DOI: <https://doi.org/10.21203/rs.3.rs-892300/v1>

License:   This work is licensed under a Creative Commons Attribution 4.0 International License.

[Read Full License](#)

INFLUENCE OF CONTROL STRATEGY IN RISK MITIGATION OF BUILDING DAMAGE DUE TO EARTHQUAKE

Normaisharah Mamat¹, Mohd Fauzi Othman², Mohd Fitri Mohd Yakub³

^{1,2,3}Department of Electronic System Engineering,
Malaysia-Japan International Institute of Technology, Universiti Teknologi Malaysia,
Jalan Sultan Yahya Petra, 54100 Kuala Lumpur, Malaysia
Email: normaisharah@utm.my

Building structures are prone to damage due to natural disasters, and this challenges structural engineers to design safer and more robust building structures. This study is conducted to prevent these consequences by implementing a control strategy that can enhance a building's stability and reduce the risk of damage. Therefore, to realize the structural integrity of a building, a hybrid control device is equipped with control strategies to enhance robustness. The control strategy proposed in this study is adaptive nonsingular terminal sliding mode control (ANTSMC). ANTSMC is an integrated controller of radial basis function neural network (RBFNN) and nonsingular terminal sliding mode control (NTSMC), which has a fast dynamic response, finite-time convergence, and the ability to enhance the control performance against a considerable uncertainty. The proposed controller is designed based on the sliding surface and the control law. The building with a two-degree-of-freedom (DOF) system is designed in Matlab/Simulink and validated with the experimental work connected to the LMSTest.Lab software. The performance of this controller is compared with those of the terminal sliding mode control (TSMC) and NTSMC in terms of the displacement response, sliding surface, and the probability of damage. The result showed that the proposed controller, ANTSMC can suppress vibrations up to 46%, and its percentage probability of complete damage is 15% from the uncontrolled structure. Thus, these findings are imperative towards increasing the safety level in building structures and occupants, and reducing damage costs in the event of a disaster.

Keywords

Control strategy. Deep learning. Collapse probability. Building damage. Enhance building safety

1. Introduction

Alleviating the structural building response in the event of an earthquake becomes an increasingly challenging task. The forces of nature threaten human existence, cause financial losses and environmental destruction. Large magnitude earthquakes damage properties and structures, and cause casualties. The earthquake magnitude of greater than 5.0 Mw may cause slight damage to the structures and buildings. The earthquake magnitude of greater than 6.0 Mw causes a lot of damage in a populated area. Moreover, major earthquakes that wreak severe damage occur at 7.0 Mw or higher. The higher moment magnitude with 8.0 Mw above will cause totally destroy to the community near the seismic location (Abu-Faraj et al. 2008). A tool known as HAZUS is used to estimate the existing building stock potential of losses caused by earthquake ground motion. HAZUS estimates the economic, physical, and social impacts of a disaster by using the geographic information system through an agency called the Federal Emergency Management Agency (FEMA). The estimation of the losses estimation is crucial for preparedness plans and rehabilitation strategies of building stocks from earthquake disasters (Duan and Pappin 2008). Besides, the HAZUS damage functions is used to simulate the vulnerability of various types of structural buildings and it provides the information on deriving the building fragility curves for various types of structures consist of the probability of slight, moderate, extensive, and complete structural damage states (Vazurkar and Chaudhari 2016; Peyghaleh et al. 2018).

Robinson et al. (2018) shows empirically derived structural fragility curves of different building types. According to the fragility curves, at 0.4 g, the building made from stone and mud has 98% probability of collapsing. The earthquake effect causes many fatalities based on the 2015 Gorkha earthquake with the recorded magnitude of 7.3 Mw to 8.8 Mw. The curves show that at the magnitude of 8.6 Mw, the number of fatalities was up to 100,000, and at the magnitude of 7.3 Mw, the earthquake caused more than 50,000 fatalities. Giordano et al. (2021) examined the fragility of the structural building made of masonry, RC frame, steel frame and timber frame. This vulnerability

48 assessment study can be adopted to assess the possible loss of Nepal's school infrastructure due to an earthquake.
49 The structural damage fragility curves can be categorized into several damage states, namely slight, moderate,
50 extensive, and complete damage. In slight damage, small plaster cracks are formed at window and door corners. In
51 the moderate state, larger cracks are formed at the window and door corners across the shear wall panel. Meanwhile,
52 in the extensive damage condition, large diagonal cracks across the shear wall panel and permanent lateral
53 movement of floors and roof are formed. Lastly, the complete damage state condition is detected by a large
54 permanent lateral displacement or imminent danger of collapse (Federal Emergency Management Agency (FEMA)
55 2003; Alam et al. 2017).

56 Ansal et al. (2010) illustrated the cumulative damage probability curve for low-rise, mid-rise and high-rise
57 reinforce concrete frame building. Other than the material of the building, the high of the building influence the
58 probability of building damage. Martins and Silva (2020) have developed an analysis on the fragility and
59 vulnerability of the most common building classes cover with the combination of structure material, height, lateral
60 load resisting system and seismic design level. Incremental dynamic analysis (IDA) is a powerful tool of seismic
61 engineering that performed to derived fragility curves for the various structures. It was developed based on the result
62 of a probabilistic seismic hazard analysis to estimate the seismic risk faced by a particular structure (Vamvatsikos
63 and Cornell 2002; Gkimprixis et al. 2020). Bayrak et al. (2021) reported that earthquake had caused severe damage,
64 partial or total collapse of many buildings. Consequently, the fatalities, livestock industry and heritage buildings are
65 affected (D'Ayala and Ansal, 2012). An earthquake warning system that delivers the ground shaking alert known
66 as earthquake early warning (EEW) can be used as a precautionary tool to provide the society to take action before
67 an incoming earthquake occurs. However, this tool has an obstacle in delivering false and missed EEW alarms
68 especially for mid and high-rise buildings due to these buildings shaking occurrence may be different from the
69 shaking at the ground (Allen and Melgar 2019; Cremen et al. 2021). Moreover, Gupta et al. (2020) mention that it
70 is difficult to predict when and where the earthquake will occur. Even if an earthquake can be predicted, the society
71 is not safe as well.

72 Therefore, innovative seismic solutions must be produced to overcome structural failures and defects. Hence,
73 structural control for buildings is needed to provide safety and more efficient designs to prevent the structures from
74 destruction. Among the structural control device, hybrid mass damper (HMD) has a prominent character that
75 combines an active mass damper and a tuned mass damper (TMD) in a control device and it is found to be cost-
76 effective by reducing energy requirement in their operation (Thenozhi and Yu 2013). Mitchell et al. (2013)
77 investigated the performance of structures by implementing HMD and other control devices. The structure has used
78 a variety of input excitations to observe the effectiveness of the control device in reducing the structural response.
79 It was found that the implementation of HMD produced better control performance than the passive device for most
80 cases. Then in 2017, Djedoui et al. (2017) investigated the hybrid control consisting of base isolator, TMD and
81 HMD to their structure system. Base isolators which are installed between the foundation and the superstructure are
82 some of the most widely used devices for vibration control. However, the floor acceleration and the inter-story drift
83 are increased, resulting in an adverse effect on the structure. The efficiency of the base isolator depends on the type
84 of excitation. A control signal required to suppress the building vibration is produced using a control algorithm
85 measured by the structural response. Based on the control signal, the actuator will generate the secondary vibration
86 response, decreasing the overall building vibration. Zamani et al. (2018) proposed adaptive fractional order fuzzy
87 proportional-integral-derivative control strategy at smart base-isolate structure to control seismic. The fuzzy rule
88 weight was adaptively tuned based on the values of the velocity of ground floor and the acceleration of the top floor.
89 The proposed control strategy had a better response in decreasing the maximum base displacement and structure
90 acceleration of the earthquake excitation given.

91 Chesne and Colette (2018) performed experimental validation of fail-safe HMD using a single DOF
92 structure. They introduced a compensator into the feedback loop by actively softening the actuator to increase the
93 stability margins of the control system. Then the same author proposed HMD to the structure system in 2017 by
94 introducing a new control law for hybrid vibration absorbers referred to as α -HMD. α -HMD requires smaller active
95 forces and less energy for the active element than the AMD and TMD (Chesné et al. 2019). In recent years, some
96 researchers were interested in the theory of finite time mechanisms. Therefore, TSMC with this characteristic is
97 introduced to overcome the problem caused by sliding mode control which involves in finite time state convergence.
98 As a result, TSMC attracts widespread attention and is known as a nonlinear switching manifold, whereas the state
99 will reach equilibrium in a finite time (Cao et al. 2013). The derivation of TSMC can be found in the study proposed
100 by Liu and Wang (2012). According to Cao et al. (2013), TSMC causes singularity to occur if the initial conditions
101 are not appropriately selected will cause an infinite control law.

Nonsingular terminal sliding mode control (NTSMC) has an advantage in giving a fast dynamic response, finite-time convergence, high control precision and eliminating the paranormal phenomenon in the control input of the system (Xu et al. 2015). NTSMC has been applied in spacecraft, vehicles and rigid manipulators to eliminate singularity problems associated with TSMC (Zhu and Yan 2014; Ning et al. 2018). In 2019, Ba et al. (2019) modified NTSMC with an adaptive time-delay estimation technique. This controller is used to track the position of servomotor-actuated robotic systems. Lastly, the proposed controller successfully verifies the servomotor robot in a real-time 2-DOF different working conditions. The collaboration of the deep learning method with NTSMC enhances the robustness of the system control, which is RBFNN that has good generalization, simple network structure, fast learning, and can improve the control performance against considerable uncertainty of the system (Liu 2013). Deep learning is a subset of machine learning methods based on artificial neural networks. In cases of earthquakes, as Xing et al. (2020) investigated, machine learning able to predict the casualties of an earthquake disaster. The technique proposed by the authors provided accurate prediction and efficient learning, making it suitable for large sample sampling and small sample data fitting. Due to the advantages of RBFNN, this technique is chosen to collaborate with NTSMC. The function of RBFNN in TSMC is to predict the upper bound of an uncertain parameter. The detailed study and the derivation of RBFNN method can be found in the studies by combined RBFNN with TSMC to control robot manipulators. This controller is used to estimate all the system parameters via Gee-Lee matrix and its produce operators. The application of ANTSMC in robot manipulators shows that the proposed controller effectively controls the nonlinear system with robustness even under model changes and parameter uncertainties.

Most of the previous studies applied this controller in the vehicle, robotic and spacecraft systems. However, there has been no empirical evidence on the influence of a control strategy in reducing the building damage risk to date. Padahal this control strategy terdiri daripada characteristic yang bagus dalam vibration control. This paper highlights the design of the newly proposed control strategy, ANTSMC and its impact in preventing the structural building from having damage and collapse by minimize the vibration during earthquake occur. This proposed control strategy integrates the deep learning technique to estimate the desired value in NTSMC. The deep learning technique has the ability to find appropriate value to fit the unknown value in the control strategy used. The proposed controller is also compared to the other controllers to demonstrate its efficiency. Moreover, the building structure representing mass, spring and damper is constructed in Simulink and validated via an experimental setup connected to LMS Test.Lab software. The result from the experimental work has strengthened the building structure that has been built in simulation.

2. System Design

2.1 Building structure

The building structure is represented by the mass, spring and damper system that consists of two DOFs. The controlling device, HMD is installed at the top floor of the building. The building structure and its free body diagram for the system is shown in Figure 1 and Figure 2, respectively. The mathematical model for the building structure are shown as (1), (2) and (3) where m_1 and m_2 denote the mass for each storey. k_1 and k_2 denote the stiffness value and while c_1 and c_2 are damping coefficients for each storey. m_d, c_d and k_d are mass, damping and stiffness for HMD. The displacement responses for each floor and the control device are defined as x_1, x_2 and x_d . \ddot{x}_g is the acceleration of the ground motion.

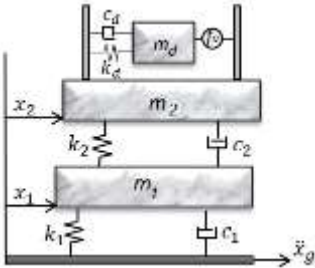


Figure 1 Building structure system for the 2-DOF system

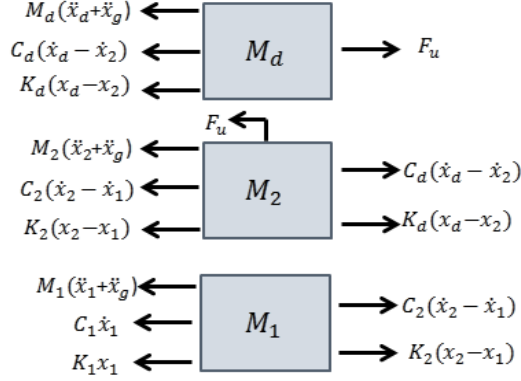


Figure 2 Free body diagram for the 2-DOF structure

148
149
150

$$M_1\ddot{x}_1 + C_1\dot{x}_1 + K_1x_1 - C_2(\dot{x}_2 - \dot{x}_1) - K_2(x_2 - x_1) = -M_1\ddot{x}_g \quad (1)$$

151
152

$$M_2\ddot{x}_2 + C_2(\dot{x}_2 - \dot{x}_1) + K_2(x_2 - x_1) - C_d(\dot{x}_d - \dot{x}_2) - K_d(x_d - x_2) = -M_2\ddot{x}_g - F_u \quad (2)$$

153
154

$$M_d\ddot{x}_d + C_d\dot{x}_d + K_dx_d - C_d\dot{x}_2 - K_dx_2 = -M_d\ddot{x}_g + F_u \quad (3)$$

155
156
157

An actuator is implemented to control HMD, and it is written as;

158
159

$$Ri + K_e(\dot{x}_d - \dot{x}_3) = F_u \quad (4)$$

160
161

$$F_u = K_f i \quad (5)$$

162
163

where \$K_f\$ is the thrust constant, \$K_e\$ is the induced voltage constant, \$R\$ is the resistance value, \$F_u\$ is the control force generated by the actuator, and \$i\$ is current.

166
167

2.2 Experimental work

168
169

The experimental work is assembled as shown in Figure 3, the assembly is consist of the shaker, amplifier, mobile Signal Conditioning and Data Acquisition System (SCADAS), accelerometer and the 2-DOF building structure. Electrodynamic exciter (S 50350/LS-120), known as shaker, generates vibrations that can be operated either in a horizontal or vertical position. In this case, the vibration of the shaker is set up to a vertical position to reproduce similar seismic movement. The power amplifier received the signal from the input and frontend into the shaker. The voltage or current required by the amplifier depends on the size of the tested system and levels of the target vibration. The accelerometer is used to measure the movement of basement and mass at each floor. The sensitivity of the accelerometer is chosen based on the maximum vibration level. SCADAS is a modular data acquisition device which consists of the frame for housing components containing all the cards, controller and power supply. The power supply includes the battery for autonomous operation, where for this model the duration of battery is around 2.5 hours. The mobile controller card is an ethernet interface linked with the Test.Lab software installed in the personal computer (PC) which consists of two output sources and two encoder inputs. SCADAS is used to capture dynamic signals, measure the accelerometer data and link the PC with Test.Lab software with amplifier. The LMS Test.Lab software was used to control the shaker and received the data from the experimental work. This software is designed as the solution for testing the equipment involved with vibration testing. It also offers quick visualization, easy reporting, and powerful analysis. It produces accurate closed-loop shaker control and has high built-in safety mechanism that reduces the risks of damaged items.

187
188

The connections between each component are illustrated in Figure 4. The input excitation for moving the shaker is generated by the software and then memorized by SCADAS. The controller card will give the signal to the amplifier and then the amplifier will generate the vibration to the shaker. Three accelerometers are placed in this study to measure the acceleration taken from the base, first floor, and second floor of the building structure. Once

189
190

191
192
193
194

the accelerometer detects the movement, the signal is sent to SCADAS DAC in acceleration value and recorded by the LMS Test.Lab software in the PC. The parameters for the experimental system parameter are shown in Table 1.

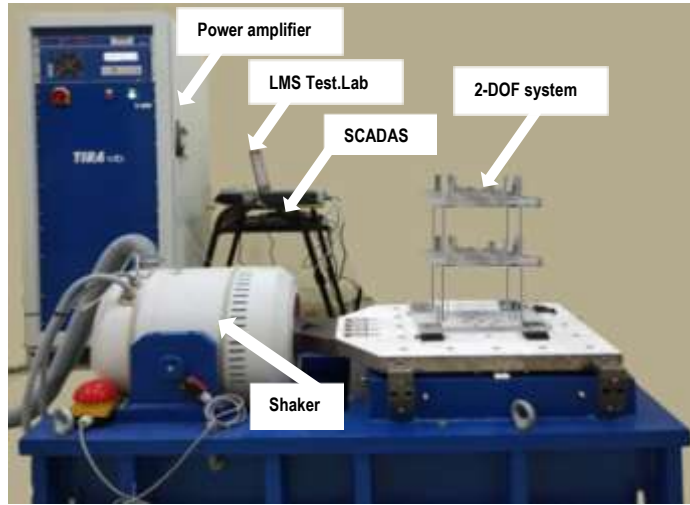


Figure 3 Experimental setup

195
196
197
198
199
200
201
202
203
204
205
206
207
208
209
210
211
212
213
214
215
216

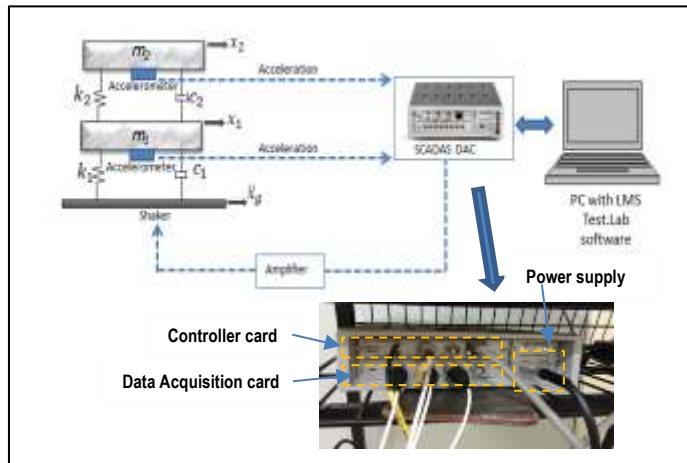


Figure 4 Experimental work connection

Table 1 Experimental system parameter

Parameter	Unit	Value
Mass (Floor 1 and 2)	kg	764.00
Stiffness (Floor 1 and 2)	n/m	182.9
Damping (Floor 1 and 2)	n.s/m	30
Accelerometer sensitivity	mV/G	10
Shaker frequency range	Hz	2-4000
Amplifier output power	VA	4200
Field voltage	V	100
Field current	A	6
Signal to noise ratio	db	> 80

217
218
219
220
221
222
223

Before running the experiment, it is required to pre-test the closed-loop system by configuring the SelfCheck setting. SelfCheck configuration is used to verify the experimental setup according to the connection, amplifier, and shaker problems. If problems occur, the status in the software window will appear "warning" or "not ok". In this case, the status showing 'Open Channel' appeared. This is because the connection between the accelerometer and data acquisition card output is not stable. The accelerometer channel did not generate a significant result above the background noise level. Other problems that occurred were caused by DAC issues while running the SelfCheck

224
225
226
227
228

configuration. The DAC issue occurs because of the situation by the shaker amplifier that has not enough output to run the full-scale equipment. The explanation of the overall process for the validation of the system is shown in Figure 5.

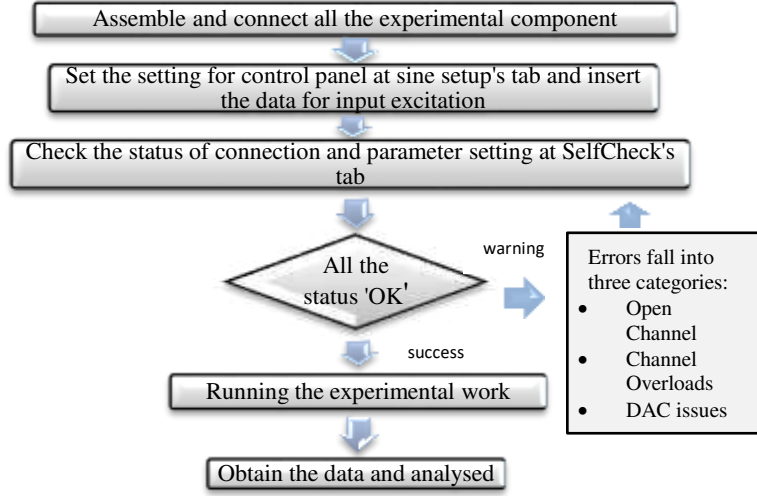


Figure 5 Flowchart of the experimental work

229
230
231
232

3. Control Strategies

233
234
235

Consider the building structure as;

236

$$\begin{cases} \dot{x}_1 = x_2 \\ \dot{x}_2 = f(x) + g(x)u + d(x) \end{cases} \quad (6)$$

237

where the system state vector, $x = [x_1, x_2, x_d]^T$, $f(x)$ and $g(x) \neq 0$ are nonlinear function of x , $d(x)$ is uncertainties and disturbance and u is the scalar control input.

238

239

240

3.1 Terminal sliding mode control

241

242

The terminal sliding surface is described as (7) where β is a design constant that must be more remarkable than 0, and the value of p and q are positive odd integers that meet the condition; $p > q$.

243

244

245

$$s = x_2 + \beta x_1^{q/p} \quad (7)$$

246

247

248

$$u = -g^{-1}(x)[f(x) + \beta \frac{q}{p} x_1^{p-1} x_2 + (l_g + \eta) \text{sgn}(s)] \quad (8)$$

249

250

where $\eta > 0$.

251

252

Stability analysis for TSMC is described as;

253

254

255

$$\dot{s} = \dot{x}_2 + \beta \frac{q}{p} x_1^{p-1} \dot{x}_1 \quad (9)$$

256

257

$$= f(x) + g(x)u + d(x) + \beta \frac{q}{p} x_1^{p-1} \dot{x}_1 \quad (10)$$

258

259

309

310

$$\dot{s} = \dot{x}_1 + \frac{1}{\beta} \frac{p}{q} x_2^{\frac{p}{q}-1} \dot{x}_2 \quad (23)$$

311

312

313

314

$$= x_2 + \frac{1}{\beta} \frac{p}{q} x_2^{\frac{p}{q}-1} (f(x) + g(x)u + d(x)) \quad (24)$$

315

316

317 Substitute equation (22) into (24) to obtain;

318

319

$$= \frac{1}{\beta} \frac{p}{q} x_2^{\frac{p}{q}-1} (d(x) - (l_g + \eta)) \quad (25)$$

320

321

$$s\dot{s} = \frac{1}{\beta} \frac{p}{q} x_2^{\frac{p}{q}-1} (sd(x) - (l_g + \eta)|s|) \quad (26)$$

322

323

$$s\dot{s} \leq -\frac{1}{\beta} \frac{p}{q} \eta x_2^{\frac{p}{q}-1} |s| \quad (27)$$

324

325

326

When $x_2 \neq 0$, $x_2^{\frac{p}{q}-1} > 0$ as to p and q are positive integers. This result in the equation (28) and it can be concluded that the condition for Lyapunov is satisfied in the case of $x_2 \neq 0$.

327

$$-\frac{1}{\beta} \frac{p}{q} \eta x_2^{\frac{p}{q}-1} > 0 \quad (28)$$

328

329 The condition when $x_2 = 0$ is studied by substituting equation (28) into (29) written as;

330

331

$$\dot{x}_2 = g(x) - \beta \frac{q}{p} x_2^{\frac{2-p}{q}} - (l_g + \eta)sgn(s) \quad (29)$$

332

333

334

335

336

337

Since we have $s > 0$, $\dot{x}_2 \leq -\eta$ and when $s < 0$, $\dot{x}_2 \geq \eta$, therefore the switching line $s = 0$ can be reach in finite time. The sliding mode $s = 0$ can be obtained from anywhere with the condition of switching trajectories in finite time.

338

3.3 Adaptive nonsingular terminal sliding mode control

339

340

341

342

343

344

345

346

347

348

349

The deep learning method, RBFNN, has the capability to approximate the uncertainties of unknown bound with universal error. Therefore, this technique is used in this study to estimate the value of the upper bound of an uncertain parameter, l_g . The structure of RBFNN is shown in Figure 6, which consists of three layers. The first layer is the input for RBFNN determined by equating the number of input variables in the process data. Five neurons in the hidden layer are the connective weight between hidden and output neurons determined using rule-of-thumb method. It is crucial to find the correct number of neurons in the hidden layer because too few neurons will result in underfitting. Underfitting occurs when a number of neurons in the hidden layer are difficult to detect the signals in a complicated data set. Meanwhile, too many neurons in the hidden layer can cause overfitting and this problem may occur when neural networks have so much information processing capacity. The steps on designing ANTSMC in this study are as follow;

350

1) Simplify the system into \dot{x}_1 and \dot{x}_2

351

2) Design sliding variables

352

3) Design NTSMC with an unknown parameter for ANTSMC, RBFNN

353

4) Perform stability analysis by satisfied Lyapunov condition

354

5) Perform analysis on attaining time

355

6) Construct in Simulink and apply to the system

356
357
358

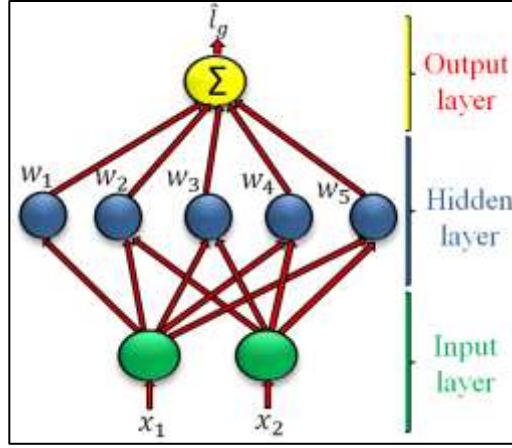


Figure 6 RBFNN structure

359
360
361
362
363

$$l_g = w^T \phi_i(x) + \vartheta_i \quad (31)$$

364

$$\phi_i(x) = \exp\left(-\frac{\|x - m_i\|^2}{\sigma_i^2}\right) \quad (32)$$

365
366

$$\hat{w} = |s|M\phi_i(x) \quad (33)$$

367 Where,

368

$$M = \frac{1}{\beta} \frac{p}{q} x_2^{\frac{p}{q}-1} \geq 0 \quad (34)$$

3.4 Controls of Structure System

369
370
371
372
373
374
375

The measurement for the sliding variable is obtained by using the mathematical model described by equations (7) and (21). The values of p and q must be positive odd numbers. After applying all the assumption values, the best performance response is obtained when the values are set to 5 and 3. The terminal sliding variables, s and control design, u for each controller used are;

376

$$s_{TSMC} = x_2 + x_1^{3/5} \quad (35)$$

377

378

$$s_{NTSMC} = x_1 + x_2^{5/3} \quad (36)$$

379

380

$$s_{ANTSMC} = x_1 + x_2^{5/3} \quad (37)$$

381

382

Theorem 1.

383

384

385

386

After applying the control law in (39) into the building structure (1), suppose that the sliding variable in (36) and (37) will converge to zero in finite time, and the proposed controller can guarantee robustness and stability of the system. The controller design for the building structure is derived as;

387

$$u_{TSMC} = k_d x_1 + c_d \dot{x}_1 - M_T \beta \frac{q}{p} x_1^{\frac{q}{p}-1} \dot{x}_2 - M_T (\xi + \eta) \operatorname{sgn}(s) \quad (38)$$

388

389

390

$$u_{NTSMC} = k_d x_2 + c_d \dot{x}_2 - M_T \beta \frac{q}{p} x_2^{2-\frac{p}{q}} - M (\xi + \eta) + \operatorname{sgn}(s) \quad (39)$$

391

392
393
394
395
396
397
398
399
400
401
402
403
404
405
406
407
408
409
410
411
412
413
414
415
416
417
418
419
420
421
422
423
424
425
426
427
428

Proof 1.

The proof for Theorem 1 is obtained through stability analysis of this controller. Consider that the Lyapunov function candidate is $V = \frac{1}{2} s^2$. Then the derivative of V along the trajectory is

$$\dot{V} = s\dot{s} \quad (40)$$

$$\dot{s} = \dot{x}_1 + \frac{1}{\beta} \frac{p}{q} x_2^{\frac{p}{q}-1} \dot{x}_2 \quad (41)$$

$$\dot{s} = x_2 + \frac{1}{\beta} \frac{p}{q} x_2^{\frac{q}{p}-1} \left[-\frac{k_T}{M} x_1 - \frac{c_T}{M} + \frac{1}{M} (u - f_d) \right] \quad (42)$$

Substitute equation (39) into (42), resulting in equation (44) as shown below; (43)

$$\dot{s} = x_2 + \frac{1}{\beta} \frac{p}{q} x_2^{\frac{p}{q}-1} \left[-\frac{k_f}{M_T} x_1 - \frac{c_f}{M_T} + \frac{f_d}{M_T} + \frac{\left[k_f x_1 + c_f x_1 - M_T \beta \left(\frac{q}{p} \right) x_2^{2-\frac{p}{q}} - M_T (\xi + \eta) \text{sgn}(s) \right]}{M_T} \right] \quad (44)$$

$$\dot{s} = x_2 + \frac{1}{\beta} \frac{p}{q} x_2^{\frac{p}{q}-1} \left[-\frac{f_d}{M_T} - \beta \left(\frac{q}{p} \right) x_2^{2-\frac{p}{q}} - (\xi + \eta) \text{sgn}(s) \right] \quad (45)$$

$$\dot{s} = -(\xi + \eta) \text{sgn}(s) - \frac{f_d}{M} \quad (46)$$

The sliding surface estimation error is written as;

$$s_e = s - \hat{s} = \hat{x}_2 \quad (47)$$

This yields equation (48), where ξ is the adaptive law value.

$$\dot{V} = s\dot{s} = (s - \hat{s} + \hat{s}) \left(-\frac{f_d}{M} - (\xi + \eta) \text{sgn}(\hat{s}) \right) \quad (48)$$

$$\dot{V} = (s - \hat{x}_2) \left(-\frac{f_d}{M} - (\xi + \eta) \text{sgn}(\hat{s}) \right) \quad (49)$$

Solve the equation above and obtain the equation as follows;

$$\dot{V} = -\frac{f_d}{M} s + \frac{f_d}{M} \hat{x}_2 - (\xi + \eta) \text{sgn}|\hat{s}| + \hat{x}_2 (\xi + \eta) \text{sgn}(\hat{s}) \quad (50)$$

Where $\frac{f_d}{M} \leq \xi$,

429

430

431

432

433

434

435

436

437

438

439

440

441

442

443

444

445

446

447

448

$$\dot{V} = \hat{s}\xi + \hat{x}_2 - (\xi + \eta)sgn|\hat{s}| + \hat{x}_2(\xi + \eta) \quad (51)$$

$$\dot{V}(t) = \dot{s}s \leq -\eta|s| \quad (52)$$

That is,

$$\dot{V} \leq -\eta|s| < 0 \text{ for } s \neq 0 \quad (53)$$

According to equation (53), the Lyapunov controller stability of ANTSMC for the building structure can be evaluated. In this study the value of η is 0.01, and the sliding surface is taken with the value of $|2 \times 10^5|$ resulted -0.02×10^5 . Therefore, the value obtained is below than 0, thus, proving that the stability of the controller, NTSMC manifold converges to zero in finite time. On the other hand, if (37) is reached, the output tracking error of the building structure will converge to zero in finite time and prove the robustness and the stability of the system. This completes the proof for Theorem 1.

This study uses two inputs, one output, and five hidden neurons. The block diagram consists of an adaptive NTSM with the building structure is shown in Figure 7, where x_f is the desired value for the system output, e is error, s is sliding mode, u is the control input, and the output feedback is displacement and velocity of the building structure.

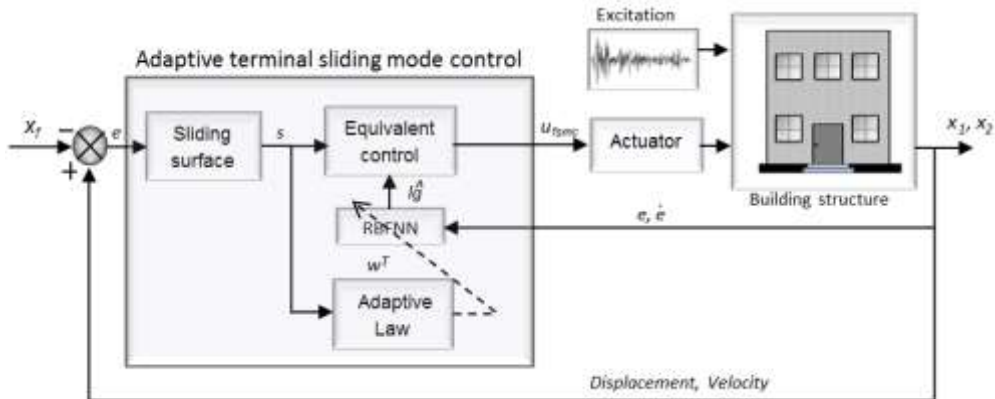


Figure 7 Block diagram of the system with the adaptive NTSMC

449

450

451

452

453

4. Result and Discussion

454

455

4.1 System validation

456

457

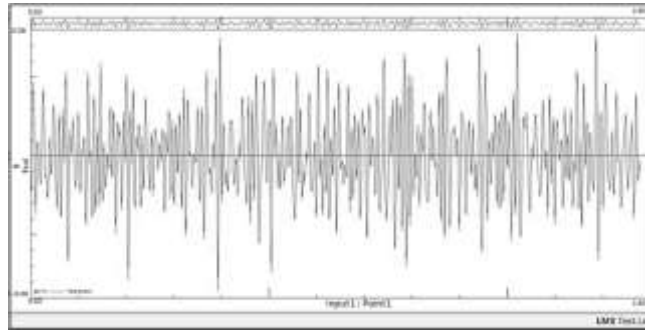
458

459

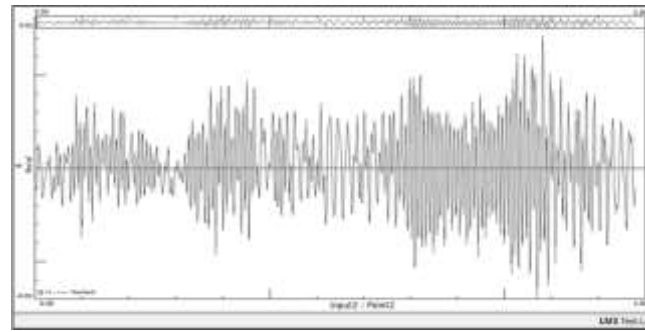
460

The building structure model constructed in Matlab are validated via an experimental setup measured by the LMS.Test lab software. The acceleration results were measured using the accelerometer as shown in Figure 8 (a), (b) and (c) for ground input, second floor and first floor with the range of 0.78 m/s², 0.01 m/s², and 0.1 m/s², respectively.

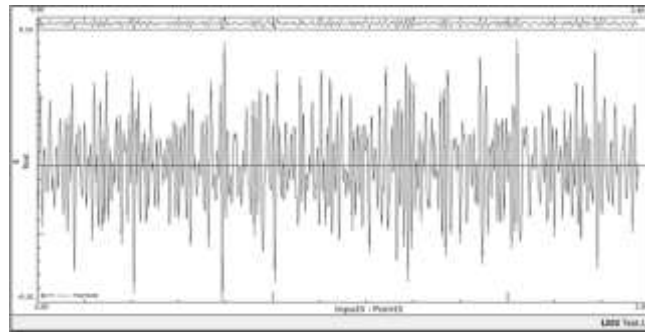
461
462
463
464



(a)



(b)



(c)

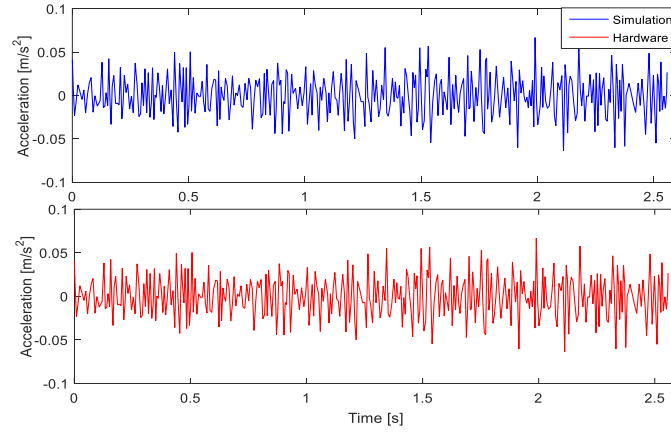
465
466
467

Figure 8 Acceleration responses measured from the experimental work (a) ground input (b) first floor (c) second floor

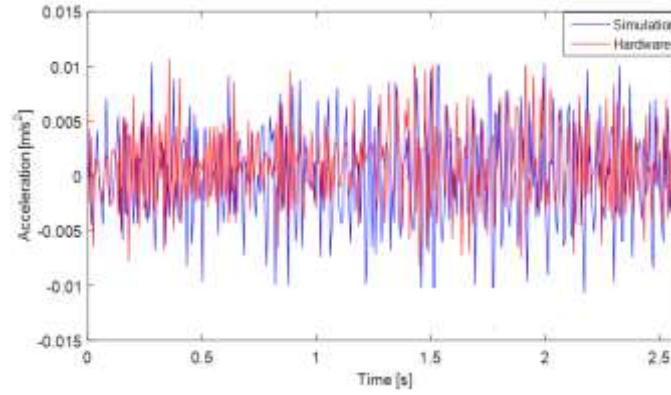
468
469
470
471
472
473
474
475
476

The results of the experimental work and simulation are compiled in Figure 9. As can be seen from these figures, the results of both methods have the same minimum and maximum values. The acceleration ranges for the first and second storeys are $\pm 0.01 \text{ m/s}^2$ and $\pm 0.1 \text{ m/s}^2$, respectively.

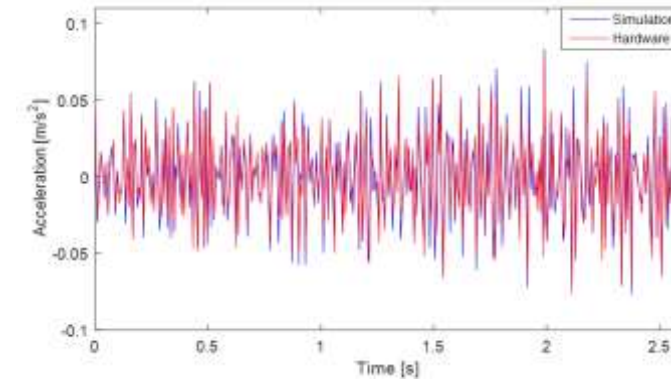
477
478



(a)



(b)



(c)

Figure 9 Comparison of the simulation and experimental results (a) ground input (b) second floor (c) first floor

479
480

481
482

483
484

485
486

4.2 Implementation of the control strategy

487
488

489
490

491
492

493
494

495
496

497
498

The building structure is equipped with HMD together with the implementation of the control strategy. The actual parameter for the building structure is used to evaluate the effectiveness of the controller in real life as shown in Table 2. Two input excitations are given as disturbances to study the robustness of the control strategy towards the system taken from the real earthquake occurred in El Centro in 1960 with the magnitude of 6.9 M_w and Southern Sumatra on 12 September 2007 with the magnitude of 8.4 M_w .

499

Number of floors	Mass (10^3kg)	Stiffness (10^5N/m)	Damping (10^5N.s/m)
First and second	320	930	15.69
HMD	44	36.7	0.71

500

501

502

503

504

505

506

507

The results obtained for the building structure with both excitations are shown in Figure 10 for the second and first floors, respectively. The result shows that the implementation of control strategies has successfully suppressed the earthquake-induced vibrations. The maximum vibration occurred at 2.17 s causing the reduction percentage measured at the second floor with respect to the uncontrolled system generated by each controller to be 46% for ANTSMC, 36% for NTSMC, and 10% for TSMC. The reduction percentage generated by the first floor is 40% for ANTSMC, 38% for NTSMC, and 7.5% for TSMC. This shows that the ANTSMC has the highest reduction percentage compared to the other controllers.

508

509

510

511

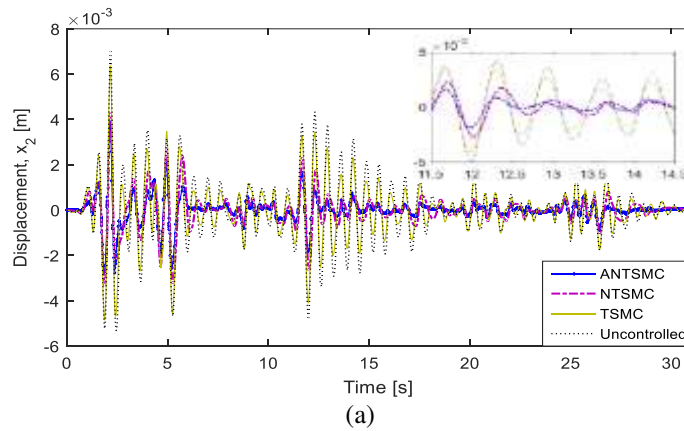
512

513

514

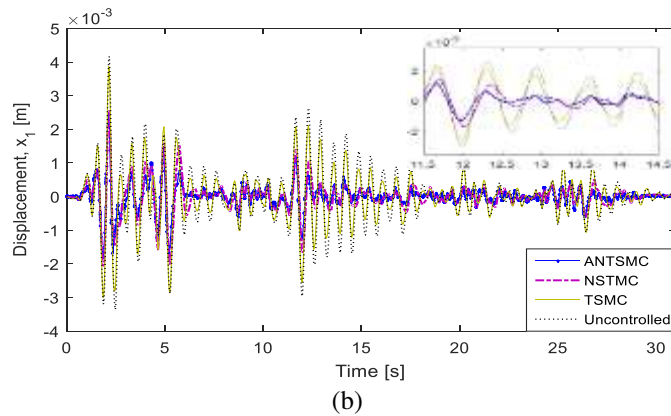
515

The second excitation taken from Southern Sumatra with the duration of acceleration is longer compared to the El Centro earthquake which is 320.725 s. The results obtained are shown in Figure 11 for both floors of the building. The maximum vibration recorded for the second and first floors are 1.3×10^{-3} m and 0.78×10^{-3} m, respectively. Based on these maximum displacement values, the percentage of vibration reduction from the uncontrolled structure for each control strategy is 42% by NTSMC, 38% by TSMC, and 19% by ANTSMC. After the implementation of control strategies, it was shown that ANTSMC has the superior performance in suppressing the building vibration.



516

517



518

519

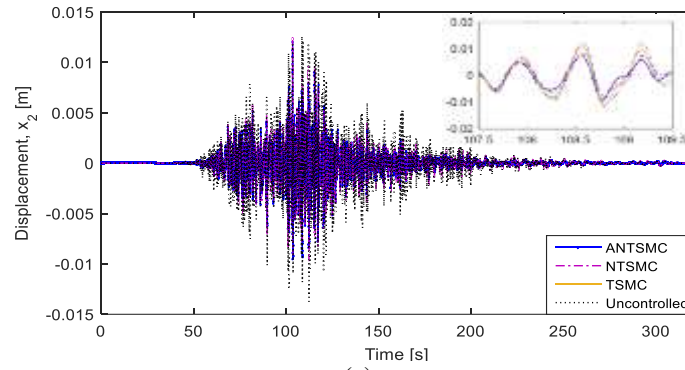
520

521

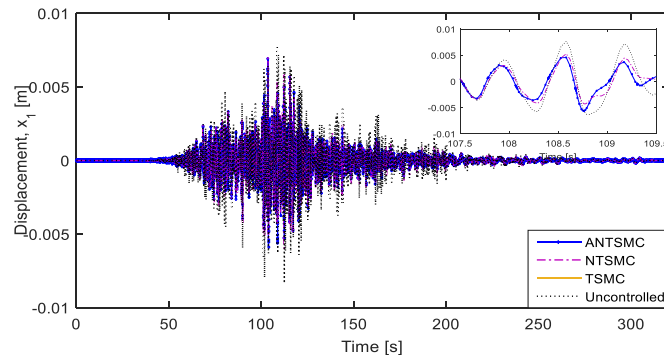
522

Figure 10 Comparison of the displacement responses for the building structure at the (a) second floor (b) first floor for the El Centro excitation

523
524



(a)



(b)

Figure 11 Comparison of the displacement responses for the building structure at the (a) second floor (b) first floor for the Southern Sumatra excitation

525
526

527
528

529

530

531

532

533

534

535

536

The sliding surface measured by the El Centro excitation for each controller is shown in Figure 12. The sliding surface design should reflect the required specification when the sliding mode is established. The figures show that the state trajectories are moving towards the sliding surface that was set to 0 to maintain the position of the system during an earthquake. This has fulfilled the system with a required response to obtain a stable condition. The same time was setting for each controller and resulting the state trajectory generated by the ANTSMC has a faster response to reach the desired sliding surface compared to NTSMC and TSMC.

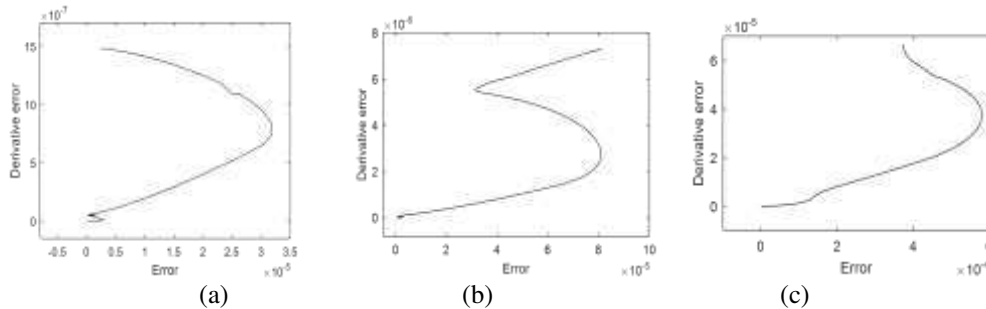


Figure 12 Sliding surface for (a) ANTSMC (b) NTSMC (c) TSMC

537

538

539

540

541

542

543

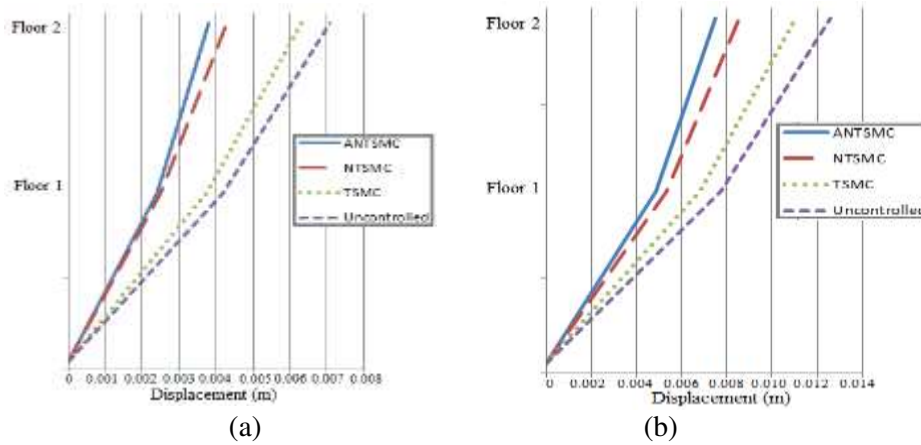
544

545

546

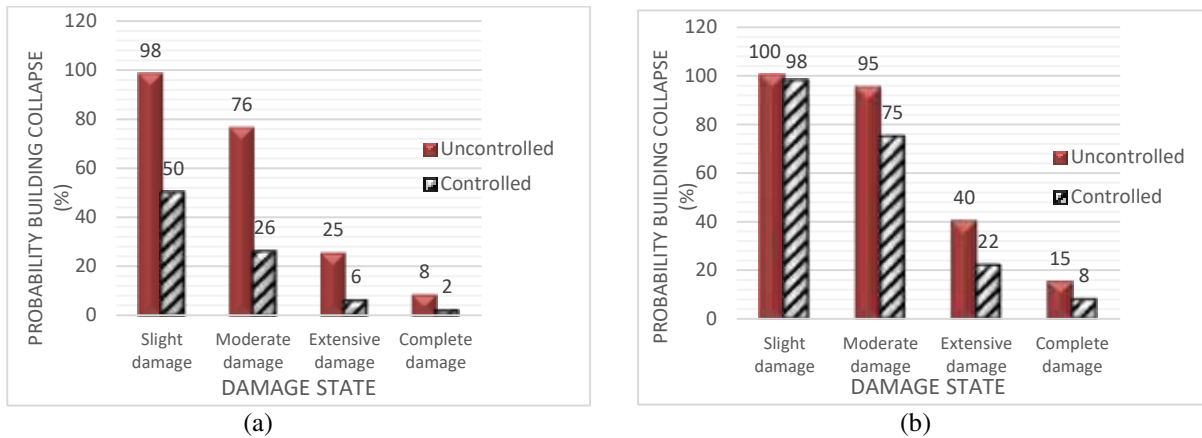
The results are summarized in Figure 13 for both excitations measured at the first and second floor taken at the maximum vibration of the building structure which occurred at 2.17 s for the El Centro and 108.6 s for the Southern Sumatra excitations. According to both figures, the second floor generated a higher sway during the seismic activity than the first floor. However, when control strategies were applied, the vibrations were suppressed.

547
548



549 Figure 13 The building response with the control strategy at each floor with the input excitations of (a) El
550 Centro (b) Southern Sumatra

551
552 This study considers the ductile reinforced concrete building and the building collapse probability is
553 measured according to the graph damage of probability for the low-rise building under the 3-DOF system according
554 to the guideline given by FAMA and IDA. Based on the probability of the building collapse for both excitations, it
555 is clear that the implementation of the proposed controller which is the adaptive NTSMC in the 2-DOF structure
556 has reduced the percentage of the building from collapse. From Figure 14 (a), the percentage of the building to have
557 slight damage is 98%, and after the implementation of the controller, the probability is reduced to 50%. Moreover,
558 the probability percentage of the building to have complete damage is reduced from 0.8% to 0.2%. From Figure 14
559 (b), the probability of the building to have slight damage is 100% which is reduced to 98%. For complete damage,
560 the probability is reduced from 15% to 0.8%. This controller shows a high percentage reduction when applied to
561 the system that is triggered by the El Centro earthquake rather than by the Southern Sumatra earthquake. However,
562 both responses show impressive results in reducing the probability of the building collapse.
563
564



565
566 Figure 14 Probability of collapse for the building structure with ANTSMC with the input excitations of (a)
567 El-Centro (b) Southern Sumatra

570 5. Conclusion

571
572 This study was aimed at investigating the influence of implementing the control strategy, namely ANTSMC to the
573 2-DOF structure in enhancing the building's structural and decreasing the risk of the building from damage. The
574 system was validated by the experimental work for the 2-DOF structure and acceleration responses were measured
575 by the LMS Test.Lab software. The result for the building system response was compared to the simulation result
576 in Simulink. ANTSMC was designed to enhance the performance of the building structure by suppressing the
577 vibration during an earthquake. The effectiveness of the controller was compared with TSMC and NTSMC. The
578

579 stability of ANTSMC was demonstrated as the building structure reached its equilibrium faster and maintained its
580 position as the desired response stated. Moreover, the proposed control strategy reduced the probability of damage
581 to the building structure. The probability percentage of the building to have slight damage with the implementation
582 of ANTSMC was reduced until 50% compared to an uncontrolled building with a probability of 98% to have a
583 slight damage. The lower percentage in having the probability of the building experiencing damage shows the
584 significant impact of the implementation of control strategy in the building structure.
585

586 **Acknowledgement**

587
588 The authors would like to acknowledge Universiti Teknologi Malaysia (research grant Professional Development
589 Research University: Q.K130000.21A2.05E38) for financially supporting this research.
590

591 **Conflict of interest**

592
593 All authors declare that they have no conflicts of interest.
594

595 **References**

- 596
597 Abu-Faraj ZO, Hamdan TF, Wehbi MR, et al (2008) The study of postural stability in an earthquake-simulated
598 environment yields a retained cognitive learning outcome. *J Biomed Pharm Eng* 2:14–21
599 Alam J, Hussan M, Sarraz A (2017) Seismic Fragility Assessment of RC Building using Nonlinear Static Pushover
600 Analysis. 26:7
601 Allen RM, Melgar D (2019) Earthquake early warning: Advances, scientific challenges, and societal needs. *Annu*
602 *Rev Earth Planet Sci* 47:361–388
603 Ansal A, Kurtuluş A, Tönük G (2010) Seismic microzonation and earthquake damage scenarios for urban areas.
604 *Soil Dyn Earthq Eng* 30:1319–1328. <https://doi.org/10.1016/j.soildyn.2010.06.004>
605 Ba DX, Yeom H, Bae J (2019) A direct robust nonsingular terminal sliding mode controller based on an adaptive
606 time-delay estimator for servomotor rigid robots. *Mechatronics* 59:82–94.
607 <https://doi.org/10.1016/j.mechatronics.2019.03.007>
608 Bayrak OF, Bikçe M, Erdem MM (2021) Failures of structures during the January 24, 2020, Sivrice (Elazığ)
609 Earthquake in Turkey. *Nat Hazards* 1–27. <https://doi.org/10.1007/s11069-021-04764-z>
610 Cao L, Chen X, Sheng T (2013) Fault tolerant small satellite attitude control using adaptive non-singular terminal
611 sliding mode
612 Chesné S, Collette C (2018) Experimental validation of fail-safe hybrid mass damper. *J Vib Control* 24:4395–4406.
613 <https://doi.org/10.1177/1077546317724949>
614 Chesné S, Inquieté G, Cranga P, et al (2019) Innovative Hybrid Mass Damper for Dual-Loop Controller. *Mech Syst*
615 *Signal Process* 115:514–523. <https://doi.org/10.1016/j.ymsp.2018.06.023>
616 Cremen G, Velazquez O, Orihuela B, Galasso C (2021) Predicting approximate seismic responses in multistory
617 buildings from real-time earthquake source information, for earthquake early warning applications. *Bull*
618 *Earthq Eng* 1–21. <https://doi.org/10.1007/s10518-021-01088-y>
619 D'Ayala D, Ansal A (2012) Non linear push over assessment of heritage buildings in Istanbul to define seismic risk.
620 *Bull Earthq Eng* 10:285–306. <https://doi.org/10.1007/s10518-011-9311-1>
621 Djedoui N, Ounis A, Pinelli JP, Abdeddaim M (2017) Hybrid Control Systems For Rigid Buildings Structures
622 Under Strong Earthquakes. *Asian J Civ Eng* 18:893–909
623 Duan X, Pappin JW (2008) A Procedure For Establishing Fragility Functions For Seismic Loss Estimate Of Existing
624 Buildings Based On Nonlinear Pushover Analysis. 14th World Conf Earthq Eng
625 Federal Emergency Management Agency (FEMA) (2003) HAZUS-MH MR4 Multi-Hazard Loss Estimation
626 Methodology – Earthquake Model: Technical Manual. Department of Homeland Security
627 Giordano N, De Luca F, Sextos A, et al (2021) Empirical seismic fragility models for Nepalese school buildings.
628 *Nat Hazards* 105:339–362. <https://doi.org/10.1007/s11069-020-04312-1>
629 Gkimprixis A, Tubaldi E, Douglas J (2020) Evaluating alternative approaches for the seismic design of structures.
630 *Bull Earthq Eng* 18:4331–4361. <https://doi.org/10.1007/s10518-020-00858-4>
631 Gupta HK, Sabnis KA, Duarah R, et al (2020) Himalayan Earthquakes and Developing an Earthquake Resilient
632 Society. *J Geol Soc India* 96:433–446. <https://doi.org/10.1007/s12594-020-1581-2>
633 Liu J (2013) Radial Basis Function (RBF) Neural Network Control for Mechanical Systems
634 <https://doi.org/10.1007/978-3-642-34816-7>

635 Liu J, Wang X (2012) Advanced Sliding Mode Control for Mechanical Systems: Design, Analysis and MATLAB
636 Simulation. Springer Science & Business Media [https://doi: 10.1007/978-3-642-20907-9](https://doi.org/10.1007/978-3-642-20907-9)
637 Martins L, Silva V (2020) Development of a fragility and vulnerability model for global seismic risk analyses. *Bull*
638 *Earthq Eng* 1–27
639 Mitchell R, Kim Y, El-Korchi T, Cha YJ (2013) Wavelet-neuro-fuzzy control of hybrid building-active tuned mass
640 damper system under seismic excitations. *JVC/Journal Vib Control* 19:1881–1894.
641 <https://doi.org/10.1177/1077546312450730>
642 Ning D, Sun S, Du H, et al (2018) Control of a multiple-DOF vehicle seat suspension with roll and vertical vibration.
643 *J Sound Vib* 435:170–191. <https://doi.org/10.1016/j.jsv.2018.08.005>
644 Peyghaleh E, Mahmoudabadi V, Martin JR, et al (2018) Impact of local site conditions on portfolio earthquake loss
645 estimation for different building types. *Nat Hazards* 94:121–150. <https://doi.org/10.1007/s11069-018-3377-x>
646 Robinson TR, Rosser NJ, Densmore AL, et al (2018) Use of scenario ensembles for deriving seismic risk. *Proc Natl*
647 *Acad Sci* 115:E9532–E9541. <https://doi.org/10.1073/pnas.1807433115>
648 Thenozhi S, Yu W (2013) Advances in modeling and vibration control of building structures. *Annu Rev Control*
649 37:346–364. <https://doi.org/10.1016/j.arcontrol.2013.09.012>
650 Vamvatsikos D, Cornell CA (2002) Incremental dynamic analysis. *Earthq Eng Struct Dyn* 31:491–514.
651 <https://doi.org/10.1002/eqe.141>
652 Xing H, Junyi S, Jin H (2020) The casualty prediction of earthquake disaster based on Extreme Learning Machine
653 method. *Nat Hazards* 102:873–886. <https://doi.org/10.1007/s11069-020-03937-6>
654 Xu W, Jiang Y, Mu C, Yue H (2015) Nonsingular terminal sliding mode control for the speed regulation of
655 permanent magnet synchronous motor with parameter uncertainties. doi: 10.1109/IECON.2015.7392393.
656 Vazurkar UY, Chaudhari DJ (2016) Development of Fragility Curves for RC Buildings. *Int J Eng Res* 5:591–594.
657 <https://doi.org/10.17950/ijer/v5i3/016>
658 Zamani A-A, Tavakoli S, Etedali S, Sadeghi J (2018) Online tuning of fractional order fuzzy PID controller in smart
659 seismic isolated structures. *Bull Earthq Eng* 16:3153–3170. <https://doi.org/10.1007/s10518-017-0294-4>
660 Zhu Z, Yan Y (2014) Space-based line-of-sight tracking control of GEO target using nonsingular terminal sliding
661 mode. *Adv Sp Res* 54:1064–1076. <https://doi.org/10.1016/j.asr.2014.05.013>
662